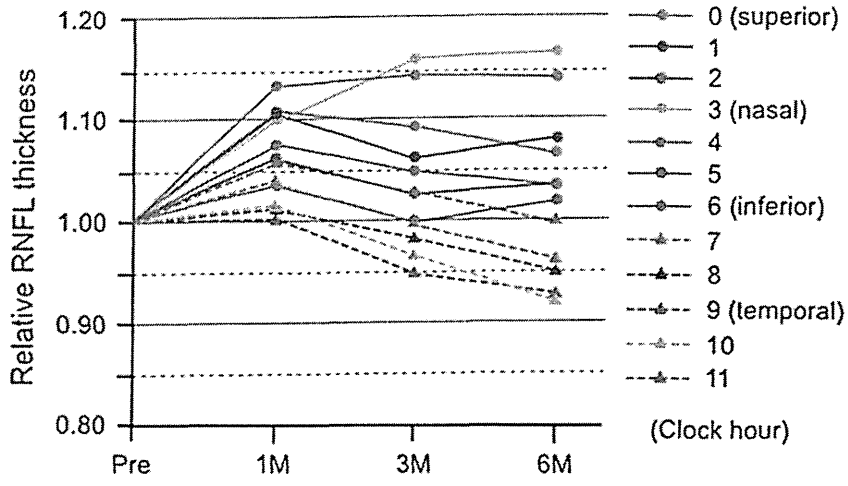

Fig. 4 Changes in the RNFL thickness before and after surgery at each of the 12 clock hours. The RNFL thicknesses are expressed relative to that before surgery. Right eye orientation was used to designate the clock hours

We suggest that the transient increase in the RNFL thickness after vitrectomy results from inner retinal damage induced during the infusion of saline and/or air that are directed against the retinal surface from the cannula during the vitrectomy. Our study showed that the transient increase in RNFL thickness was statistically significant at nasal, upper and lower regions, especially the 0–5 clock hour regions, where the saline and/or air was directed from the infusion cannula. We also believe that saline-induced stress, as well as air, is involved in the transient increase in RNFL thickness because Tsuiki et al. [18] reported that epiretinal membrane removal vitrectomy without air–fluid exchange also causes a transient increase of RNFL thickness.

The time course of the changes in the RNFL thickness after MH surgery depended on the retinal regions. At the 3 and 4 clock hours, the RNFL remained thicker than the pre-treatment level up to 6 months, but at other regions, the RNFL thickness returned to the pre-surgery level or decreased to be thinner than that of the pre-surgery level (Fig. 4). We do not know the exact cause of this different pattern of RNFL thickness at different retinal regions, but this may be due to different degrees of inner retinal damage in the different retinal regions. Long-term follow-up of RNFL thickness after MH surgery or animal experiments may be useful to clarify this question.

We cannot explain why the temporal quadrant of the RNFL thickness did not show the transient increase (Fig. 2). However, the ILM peeling was performed in this area of the nerve fiber layer that feeds this quadrant, and the damage due to the ILM peeling may not be so severe as to cause the transient edema of the RNFL. Another possibility might be that the RNFL damage due to ILM peeling might cause a gradual decrease of the RNFL thickness at a relatively later period after the surgery without any early RNFL increase as seen in Fig. 3.

There are two limitations in this study. The first limitation was that we analyzed the RNFL thickness only in a circle around the optic disc with a diameter of 3.46 mm, and did not measure the RNFL in more peripheral retinal areas. Recent advances in the mapping of the RNFL thickness or ganglion cell complex analysis may provide more useful information. The second limitation was the short follow-up period. We followed the RNFL thickness for 6 months, but the RNFL thickness was still not stabilized at this time. It would be interesting to see how the RNFL thickness at each region changes and stabilizes during the one and 2 years after surgery.

Conclusions

Our results showed that there was a transient increase in the peripapillary RNFL thickness after MH surgery. The increase in the RNFL thickness in the early stages after surgery is probably caused by a slight edema of inner retinal layer caused by the MH surgery.

Acknowledgments The authors thank Duco I. Hamasaki for editing the manuscript. Grant-in-Aid for Scientific Research B (#203904480 HT), and C (#20592075 MK) from Ministry of Education, Culture, Sports, Science and Technology (http://www.jsps.go.jp/).

Conflict of interest The authors declare that they have no conflict of interests.

References

1. Kelly NE, Wendel RT (1991) Vitreous surgery for idiopathic macular holes. Results of a pilot study. Arch Ophthalmol 109:654–659
2. Yooh HS, Brooks HL Jr, Capone A Jr et al (1996) Ultrastructural features of tissue removed during idiopathic macular hole surgery. Am J Ophthalmol 122:67–75
3. Park DW, Sipperley JO, Sneed SR et al (1999) Macular hole surgery with internal-limiting membrane peeling and intravitreous air. Ophthalmology 106:1392–1397
4. Gaudric A (2009) Macular hole sugery. Simple or complex? Am J Ophthalmol 147:381–383
5. Melberg NS, Thomas MA (1995) Visual field loss after pars plana vitrectomy with air/fluid exchange. Am J Ophthalmol 120:386–388
6. Hutton WL, Fuller DG, Snyder WB et al (1996) Visual field defects after macular hole surgery: a new finding. Ophthalmology 103:2152–2158
7. Boldt HC, Munden PM, Folk JC, Mehaffey MG (1996) Visual field defects after macular hole surgery. Am J Ophthalmol 122:371–381
8. Bopp S, Lucke K, Hille U (1997) Peripheral visual field loss after vitreous surgery for macular holes. Graefes Arch Clin Exp Ophthalmol 235:362–371
9. Ezra E, Arden GB, Riordan-Eva P et al (1996) Visual field loss following vitrectomy for stage 2 and 3 macular holes. Br J Ophthalmol 80:519–525
10. Pendergast SD, McCuen BW 2nd (1996) Visual field loss after macular hole surgery. Ophthalmology 103:1069–1077
11. Welch JC (1997) Dehydration injury as a possible cause of visual field defect after pars plana vitrectomy for macular hole. Am J Ophthalmol 124:698–699
12. Hirata A, Yonemura N, Hasumura T et al (2000) Effect of infusion air pressure on visual field defects after macular hole surgery. Am J Ophthalmol 130:611–616
13. Ueno S, Kondo M, Piao CH et al (2006) Selective amplitude reduction of the PhNR after macular hole surgery: ganglion cell damage related to ICG-assisted ILM peeling and gas tamponade. Invest Ophthalmol Vis Sci 47:3545–3549
14. Ebisawa N, Mori K, Yoneya S (2000) Thickness of retinal nerve fiber layer decreases after vitreous surgery for idiopathic macular hole. Nihon Ganka Gakkai Zasshi (Japanese) 104:142–147
15. Yamashita T, Uemura A, Kita H, Sakamoto T (2006) Analysis of the retinal nerve fiber layer after indocyanine green-assisted vitrectomy for idiopathic macular holes. Ophthalmology 113:280–284
16. Brazitikos PD, Katsimpris JM, Tsironi E, Androudi S (2010) Retinal nerve fiber layer thickness evaluation after trypan blue-assisted macular surgery. Retina 30:640–647
17. Tsuiki E, Koga M, kitaoka T (2007) Changes in retinal nerve fiber layer thickness following vitreous surgery. Rinsho Ganka (Japanese) 61:357–360
18. Tsuiki E, Kusano M, Kishikawa Y, Kitaoka T (2008) Changes in the thickness of retinal nerve fiber layer after vitreous surgery for macular hole or epiretinal membrane. Rinsho Ganka (Japanese) 61:347–350
19. Gass JD (1988) Idiopathic senile macular hole: its early stages and pathogenesis. Arch Ophthalmol 106:629–639
20. Gass JD (1995) Reappraisal of biomicroscopic classification of stages of development of a macular hole. Am J Ophthalmol 119:752–759
21. Nassif N, Cense B, Park BH et al (2004) In vivo human retinal imaging by ultrahigh-speed spectral-domain optical coherence tomography. Opt Lett 29:480–482
22. Gandorfer A, Haritoglou C, Gass CA et al (2001) Indocyanine green-assisted peeling of the internal limiting membrane may cause retinal damage. Am J Ophthalmol 132:431–433
23. Gandorfer A, Haritoglou C, Gandorfer A, Kampik A (2003) Retinal damage from indocyanine green in experimental macular surgery. Invest Ophthalmol Vis Sci 44:316–323
24. Haritoglou C, Gandorfer A, Gass CA et al (2002) Indocyanine green-assisted peeling of the internal limiting membrane in macular hole surgery affects visual outcome: a clinicopathologic correlation. Am J Ophthalmol 134:836–841
25. Horio N, Horiguchi M (2004) Effect on visual outcome after macular hole surgery when staining the internal limiting membrane with indocyanine green dye. Arch Ophthalmol 122:992–996
26. Ando F, Yasui O, Hirose H, Ohba N (2004) Optic nerve atrophy after vitrectomy with indocyanine green-assisted internal limiting membrane peeling in diffuse diabetic macular edema: adverse effect of ICG-assisted ILM peeling. Graefes Arch Clin Exp Ophthalmol 242:995–999

Vision Research 91 (2013) 118–123

Contents lists available at ScienceDirect

Vision Research

journal homepage: www.elsevier.com/locate/visres

Focal cone ERGs of rhodopsin Pro347Leu transgenic rabbits

Shinji Ueno [a,*], Toshiyuki Koyasu [a], Taro Kominami [a], Takao Sakai [a], Mineo Kondo [b], Shunsuke Yasuda [a], Hiroko Terasaki [a]

[a] Department of Ophthalmology, Nagoya University Graduate School of Medicine, Nagoya, Japan
[b] Department of Ophthalmology, Mie University Graduate School of Medicine, Tsu, Japan

ARTICLE INFO

Article history:
Received 21 May 2013
Received in revised form 9 August 2013
Available online 21 August 2013

Keywords:
Focal ERG
Retinal degeneration
Transgenic rabbit
Retinitis pigmentosa
Oscillatory potentials
Inner retina

ABSTRACT

A rhodopsin P347L transgenic (Tg) rabbit, a model of retinitis pigmentosa, has been generated in our laboratory. The purpose of this study was to determine the properties of focal areas of the retina in this rabbit model during the course of retinal degeneration. To accomplish this, we recorded focal ERGs from wild-type (WT) and Tg rabbits at ages 3, 6, and 12 months. A 15° stimulus spot was used to elicit the focal ERGs from the center of the visual streak and from four surrounding areas. We found that the amplitudes of the focal cone ERG b-waves and oscillatory potentials (OPs) of the Tg rabbits in the five areas decreased progressively with increasing age and became almost non-recordable at 12 months. There were no significant regional differences in the b-waves of Tg rabbits recorded from the 5 areas. The amplitudes of the OPs were better preserved than the b-waves and the OPs/b-wave ratio was higher than that in WT rabbits at every recording area. The summed OPs amplitudes, which most likely originate from the amacrine and/or ganglion cells, recorded from the area superior to the optic disc was significantly larger than that from other areas at 3- and 6-months-old. This indicated that the inner retinal neurons were not altered equally after photoreceptor degeneration in this rabbit model.

1. Introduction

Retinitis pigmentosa (RP) is a group of inherited retinal diseases caused by mutations of genes related to the retina. These mutations result in degeneration of the rod photoreceptors followed by a gradual loss of cones. Photoreceptor degeneration is followed by the death of the inner retinal cells (Heckenlively, 1988; Weleber, Gregory-Evance, et al., 2006). The retinal degeneration usually begins in the periphery, and the function and morphology of cone-rich central area are relatively well preserved until the late stages of the disease process.

Different subjective and objective examinations have been used to assess the macular function in patients with RP. Among the objective methods, focal ERGs (Ikenoya et al., 2007; Sugita et al., 2008) and multifocal ERGs (Chan & Brown, 1998; Hood et al., 1998; Seeliger et al., 1998; Vajaranant et al., 2002) have been used. Our laboratory has developed a technique for recording focal cone ERGs while monitoring the location of the stimulus on the fundus with an infrared camera during the recordings (Kondo et al., 2008; Miyake, 1990; Miyake et al., 1989; Shiroyama & Miyake, 1990). In our system, focal ERGs can be recorded even in patients without good fixation, and the a- and b-waves and oscillatory potentials (OPs) elicited by focal stimuli resemble full-field cone ERGs.

To study the pathophysiology of RP, we have generated a rhodopsin P347L transgenic (Tg) rabbit using bacterial transgenes (Kondo et al., 2009). We found that the rod function of Tg rabbits was reduced at an early age whereas the cone function was relatively well preserved. We also noted that the oscillatory potentials (OPs), which are believed to originate mainly from amacrine and ganglion cells (Dong, Agey, & Hare, 2004; Wachtmeister, 1998), were larger than those of wild type rabbits (Sakai et al., 2009). Although the exact mechanism(s) underlying these secondary changes in the postreceptoral neurons has not been fully determined, our results indicated that the activities of the inner retinal neurons were altered in Tg rabbits (Marc et al., 2007).

The visual streak of the rabbit retina is a horizontal band lying inferior to the optic nerve head where the densities of rods and cones are higher than elsewhere in the retina (Famiglietti & Sharpe, 1995; Juliusson et al., 1994) Our histopathological study of Tg rabbits showed that the retinal degeneration developed earlier in the visual streak than in other areas (Kondo et al., 2009).

The conclusions made from these earlier ERG studies were mainly based on the results obtained from full-field ERGs, and we do not know whether there are local functional changes in the retina in this rabbit model. Thus, the purpose of this study was to determine the characteristics of local areas of the retina of Tg rabbits by recording focal ERGs. To accomplish this, we

* Corresponding author. Address: 65 Tsuruma-cho, Showa-ku, Nagoya 466-8550, Japan. Fax: +81 52 744 2278.
E-mail address: ueno@med.nagoya-u.ac.jp (S. Ueno).

0042-6989/$ - see front matter © 2013 Elsevier B.V. All rights reserved.
http://dx.doi.org/10.1016/j.visres.2013.08.006

recorded and analyzed the changes in the b-waves and the OPs from 5 regions of the retina of Tg rabbits at 3, 6, and 12 months.

2. Materials and methods

2.1. Animals

The experiments were performed on 8 Tg and 9 wild type (WT) pigmented rabbits whose ages ranged from 3 to 12 months. After recording the ERGs, 1 Tg rabbit was euthanized at 3 months, and 3 WT and 3 Tg rabbits were euthanized at 6 months. All protocols were approved by the Institutional Review Board of Nagoya University Graduate School of Medicine and adhered to the EU Directive 2010/63/EU for animal experiments.

The techniques used for generating the Tg rabbits has been described in detail (Kondo et al., 2009). We used pigmented rabbits, a cross of Dutch pigmented rabbits and New Zealand albino rabbits because the stray light effects are lower in pigmented eyes. The animals were anesthetized with an intramuscular injection of 25 mg/kg ketamine and 2 mg/kg xylazine to record the ERGs.

2.2. Stimuli for focal ERGs

The system for recording focal ERGs consisted of a modified infrared fundus camera and an electronic pulse generator that controlled the light-emitting diodes (LEDs) used for the stimulus and background illumination (Kowa, Nagoya, Japan). An infrared television fundus camera was modified so that the stimuli were presented in Maxwellian view. The images from this fundus camera were fed to a television monitor with a 45° view of the posterior pole of the eye. The position of the stimulus spot on the fundus was monitored on the television screen and could be moved by the examiner with a joystick. A white LED was used for the stimulus and background illumination that covered a retinal area of 45°. The size of the stimulus spot was 15°, and the luminance of the background was fixed at 3 phot cd/m^2 for photopic conditions. The luminance of the stimulus spot was 30 phot cd/m^2, and the stimulus duration was 100 ms for photopic conditions. The luminance of the stimulus spot was 3 phot cd/m^2 and the stimulus duration was 10 ms for scotopic conditions. The stimulus repetition rate was fixed at 2 Hz. The luminance of the stimulus and background illumination was measured at the corneal surface and then converted to the value at the retinal surface. These luminances were measured with a photometer (Model IL 1700; International Light, Newburyport, MA).

2.3. Focal ERG recordings

The cornea was anesthetized with topical 1% tetracaine, and the pupils were dilated with topical 0.5% tropicamide and 0.5% phenylephrine HCl. The ERGs were recorded with a Burian-Allen bipolar contact lens electrode (Hansen Ophthalmic Development Laboratories, Iowa City, IA), and the ground electrode was attached to the ipsilateral ear. The responses were amplified, and the band pass filters were set at 0.5 to 1000 Hz. The ERGs were digitized at 5 kHz, and 500 responses were averaged (MEB-9100 Neuropack; Nihon Kohden, Tokyo, Japan).

To confirm that the stimulus and recording conditions elicited focal ERGs, we investigated the effect of stray light on the responses. We made an approximately 15° laser scar on the visual streak to two other WT pigmented rabbits (Fig. 1A), and we recorded the focal ERGs elicited by stimulating the visual streak and the photocoagulated area.

A fundus photograph of a 3-months-old WT rabbit is shown in Fig. 2, and the gray ellipse shown below the optic disc outlines the

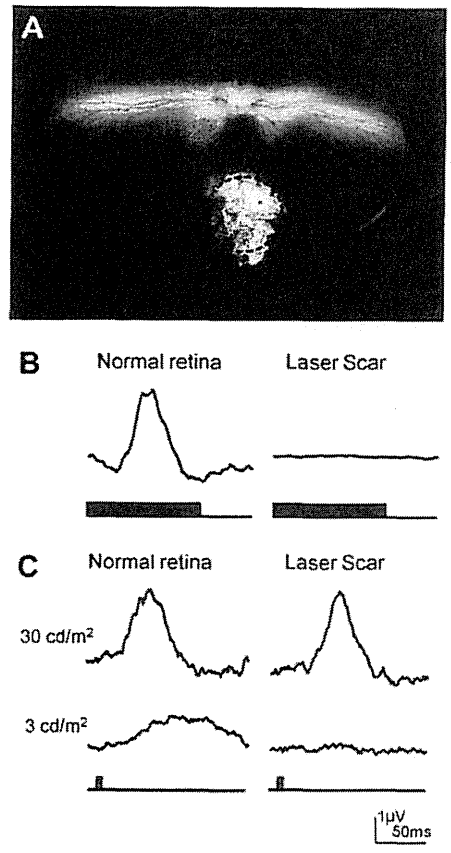

Fig. 1. Experiments to determine whether the focal ERGs arise from only the stimulated area. (A) Fundus photograph showing laser scar in the visual streak of a wild rabbit. Dotted circular indicates the area of stimulation to elicit focal ERGs. (B) Focal cone ERGs from normal retina (visual streak) and laser scar ERGs were recorded with a 3 cd/m^2 steady background. The luminance of the stimulus spot was 30 phot cd/m^2, and the stimulus duration was 100 ms. The focal ERGs were almost non-recordable from the area photocoagulated. (C) Focal rod ERGs from normal retina (visual streak) and laser scar. ERGs were recorded without background light. The ERGs recorded with stimulus intensity of 30 cd/m^2 with 10 ms duration are shown in the upper row. ERGs were recorded even from the area photocoagulated due to stray light. The ERGs recorded with stimulus intensity of 3 cd/m^2 with 10 ms duration are shown in the lower row. The focal ERGs were almost non-recordable from the area photocoagulated.

visual streak (Famiglietti & Sharpe, 1995; Juliusson et al., 1994). To compare the local retinal function of Tg and WT rabbits, we recorded ERGs from 5 areas of the retina as shown in Fig. 2. The ERGs were elicited by a 15° stimulus spot placed superior to the disc (A), nasal to the visual streak (B), center of the visual streak (C), temporal to the visual streak (D), and inferior to the visual streak (E).

2.4. Measurement of b-wave and OPs

The amplitudes of the b-waves and OPs were measured by a masked researcher. The amplitude of the b-wave was measured from the bottom of the negative a-wave to the top of the positive wave (Fig. 2, lower). To determine the appropriate band pass filters for isolating the OPs of WT and Tg rabbits, we first analyzed the ERGs by Fast Fourier Transform (FFT) as reported (Sakai et al., 2009). Based on the results, we chose band pass settings of 50–300 Hz for isolating the focal OPs (Fig. 2, lower). We measured the amplitude of each OP wavelet from the trough to the peak of the filtered waveforms, and one masked researcher checked the original waveform and decided on the position of the trough and peak of each OP. When a clear oscillation could not be found, we

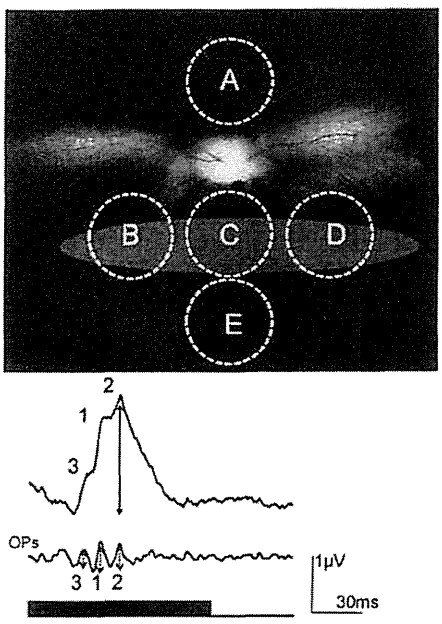

Fig. 2. Fundus panorama of left eye of a 3-months-old WT rabbit (upper). White ellipse inferior to the optic disc indicates the location of the visual streak. We recorded focal ERGs using a 15° stimulus spots from the 5 areas. (A) Superior to the optic disc. (B) Nasal on the visual streak. (C) Center of visual streak. (D) Temporal on the visual streak. (E) Ventral of the visual streak. Representative focal ERGs of WT rabbit (lower). Upper trace is the original waveform and the extracted OPs are in the middle. Stimulus markers are at the bottom. Arrow in the original wave shows the amplitude of the b-wave. The OPs consists of several wavelets; 1 is the largest OP, 2 is the second largest, and 3 is the third largest. We analyzed the sum of the amplitudes of 1, 2, and 3.

set the amplitude to zero. We used the sum of the 3 largest OP wavelets (1, 2, and 3) because each OP was too small to analyze separately.

2.5. Retinal histology

To examine the histological changes of the retina, 3 eyes of 6-months-old Tg and WT rabbits were evaluated. The rabbit eyes were fixed overnight in a mixture of 10% neutral buffered formalin and 2.5% glutaraldehyde then transferred to 10% neutral buffered formalin. The tissues were trimmed, embedded in paraffin, sectioned vertically through the optic nerve (superior-inferior), and stained with hematoxylin and eosin. Retinal sites 4 mm superior to the optic disc, 2 mm and 6 mm inferior to the optic disc were evaluated. These sites were presumed to be the center of the focal ERG stimulus at the superior, center, and inferior to the optic disc (Fig. 2 upper). The thickness of the inner retina from the inner limiting membrane to the outer plexiform layer, and the outer nuclear layer (ONL) was measured.

2.6. Statistical analyses

The data were analyzed with the SPSS computer software. The amplitude of the b-wave and sum OPs were compared with *t*-tests or multiple comparisons. A difference was considered statistically significant when $P < 0.05$.

3. Results

3.1. Assessing recording conditions

To confirm that our focal ERGs were responses only from the stimulated site of the retina and not from other sites stimulated by stray light, we made an approximately 15° laser scar on the visual streak of two WT rabbits (Fig. 1A). We then recorded focal ERGs from the normal visual streak and from the area of the laser photocoagulation with a 15° spot under both photopic and scotopic conditions. We determined the appropriate stimulus conditions for recording focal ERG for WT rabbits initially. For the photopic condition, we used a stimulus with a luminance of 30 cd/m^2 with 100 ms duration presented on a 3 cd/m^2 steady background. We found that the focal ERGs from laser scar were below the noise level of the recordings (Fig. 1B) and concluded this stimulus setting was appropriate for recording focal cone ERGs. Next we determined the conditions for recording focal rod ERGs. We found that stimuli of 30 cd/m^2 with 10 ms duration imaged on the laser scar elicited ERGs after 15 min dark-adaptation. We assumed that the responses originated from stray light (Fig. 1C), and we reduced the stimulus intensity and found that stimulus intensity of 3 cd/m^2 and 10 ms duration did not elicit a response when it was imaged on the laser scar. We then used these stimulus parameters to study the focal rod ERGs (Fig. 1C).

3.2. Focal cone ERGs from wild type (WT) rabbits

Focal cone ERGs were recorded from the 5 retinal areas of 6 WT rabbits at 3 and 6 months. Representative focal cone ERGs elicited from areas A to E of a 3-months-old WT rabbit are shown in the left row of Fig. 3. The isolated OPs are shown below each of the ERGs. The focal cone ERGs from each site were similar in shape and consisted of a small negative a-wave followed by a large positive b-wave with the OPs superimposed on the b-wave. The mean ± SEM amplitudes of the b-waves of the focal ERGs at 3 and 6 months are plotted on the left side of Fig. 4 (black bars). At 3 months, the b-wave of area C was significantly larger than that of areas A and E ($C = 3.1 \pm 1.0$ μV; $A = 2.3 \pm 1.2$ μV; $E = 2.3 \pm 1.0$ μV; $P < 0.05$; paired *t*-tests). The means ± SEM amplitudes of the sum of the OPs at 3 and 6 months WT rabbits ($n = 6$ each) are plotted on the right side of Fig. 4. The amplitudes of the OPs varied considerably among the rabbits, and the differences in the amplitudes among the 5 areas (minimum = 0.7 ± 0.1 μV at B; maximum = 1.1 ± 0.2 μV at A at 3 months; multiple comparisons) were not significant. We also compared the focal cone ERGs of 3- and 6-months-old WT rabbits. The amplitudes of the b-waves from each area of 6-months-old WT rabbit was slightly smaller than that of 3–months-old rabbits, but the differences between the amplitudes at the two ages in each area were not significant (paired *t*-tests).

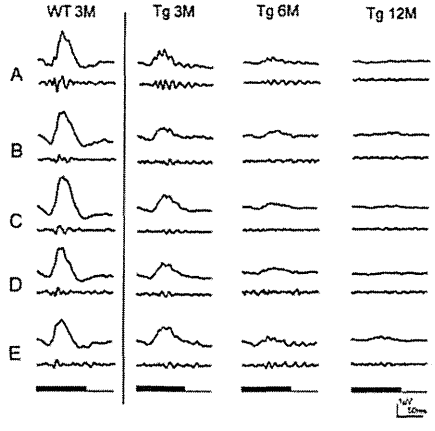

Fig. 3. Representative focal cone ERGs recorded from the 5 areas designated in Fig. 2. For ERGs of a WT rabbit at 3 months and of Tg rabbits at 3, 6, and 12 months are shown. The focal cone ERGs of the Tg rabbits decreases with increasing age. The OPs from area A is larger than those from other areas in the 3-months-old Tg rabbit.

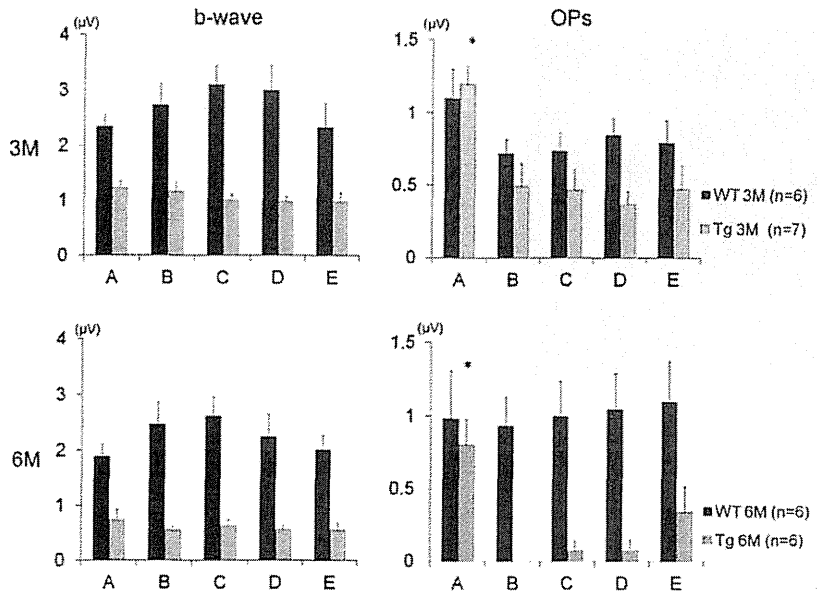

Fig. 4. Amplitudes of b-wave and OPs from 5 areas of WT and Tg rabbits (mean + SEM). Amplitudes of focal ERG b-wave at 3-months-old are shown in the upper left, and the sum of focal ERG OPs at 3-months-old are shown in the upper right. Amplitudes of the focal ERG b-waves at 6-months-old are shown in the lower left, and the amplitudes of sum of focal ERG OPs at 6-months-old are shown in the lower right. The amplitude of OPs in area A was significantly larger than that in other areas in Tg rabbit (*$P < 0.05$).

3.3. Focal cone ERGs of Tg rabbits

Focal cone ERGs were recorded from 7 Tg rabbits at 3 months, 6 Tg rabbit at 6 months and 3 Tg rabbits at 12 months. Representative ERGs of one Tg rabbit recorded at 3, 6, and 12 months are shown in Fig. 3. The amplitudes of the ERGs progressively decreased with increasing age and were almost non-recordable at 12 months. The OPs from the superior area (A) were distinguishable at 3 months. The amplitudes of b-waves in the Tg rabbits were significantly smaller than that of WT rabbits at each recording area (Fig. 4 left, gray bars). The means ± SEMs of the amplitude of the b-waves at 6 months were significantly reduced in area A (0.7 ± 0.2 μV), area B (0.6 ± 0.1 μV), area C (0.6 ± 0.1 μV), area D (0.6 ± 0.1 μV), and area E (0.6 ± 0.2 μV) than that at 3 months (A = 1.2 ± 0.1 μV; B = 1.2 ± 0.2 μV; C = 1.0 ± 0.1 μV; D = 1.0 ± 0.1 μV; E = 1. 0 ± 0.2 μV; $P < 0.05$, *t*-tests for all areas). However, the differences in the amplitudes of the b-waves in the 5 areas were not significant at 3 and 6 months.

At 3 months, the amplitudes of the OPs were better preserved than the b-waves, and the OPs/b-wave ratio was higher than that in WT rabbits at every recording area. The sum of the OPs at area A (1.2 ± 0.1 μV) was best preserved, and the sum was significantly larger than that of other areas (B = 0.5 ± 0.2 μV; C = 0.5 ± 0.2 μV; D = 0.4 ± 0.1 μV; E = 0.5 ± 0.2 μV; $P < 0.05$, multiple analyses; Fig. 4). At 6 months, the OPs became undetectable in most of the Tg rabbits at areas B, C, and D. However at area A, the OPs were still prominent, and the amplitude was significantly larger than that at the other recording areas (0.8 ± 0.2 μV; $P < 0.05$, multiple analysis). At 12 months, the focal cone ERGs of the 3 Tg rabbits became almost non-recordable at all sites.

3.4. Focal rod ERGs of WT and Tg rabbits

Focal rod ERGs were recorded from the 5 retinal areas of 2 Tg and 2 WT rabbits at 3 months. Representative ERGs from a Tg and a WT rabbit are shown in Fig. 5. The focal rod ERGs from each site were similar in shape which had small positive b-wave but no a-wave and OPs. The amplitudes of b-wave of WT rabbit were approximately 1.2 μV at all 5 areas. On the other hand, the focal rod ERGs of Tg rabbit were non-recordable even at 3 months.

3.5. Retinal histology

The retinal sections of the area of superior to disc (A), center of the visual streak (C), ventral of visual streak (E) of a WT rabbit and a Tg rabbit at 6 months are shown in the upper half of Fig. 6. It is known that in normal rabbits, the density of rods and cones is highest at the visual streak. Consistent with previous reports (Famiglietti & Sharpe, 1995), the thickness of the ONL in WT rabbits was maximum at the visual streak (Fig. 6 lower right). There were regional differences in the degree of photoreceptor loss in the Tg rabbits (Kondo et al., 2009). Only a single row of nuclei remained in the ONL at the center of the visual streak (C) and the thickness of the ONL at the visual streak was reduced relatively more than the two other locations (Fig. 6 lower right). In contrast, the thickness of the inner retina was well preserved at 6 months. The thickness of inner retina was almost same as that of control. From retinal histology of hematoxylin and eosin stained retinas, it was difficult to detect any inner retinal change which could have caused the abnormal OPs responses dorsal to the disc (A).

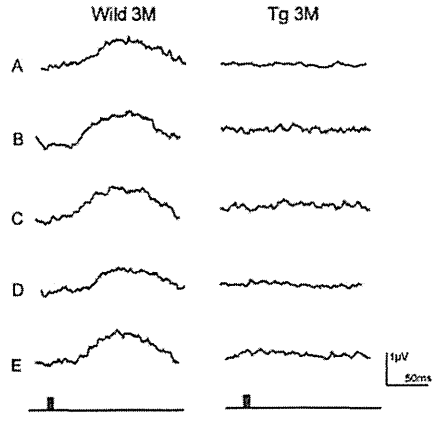

Fig. 5. Representative focal rod ERGs recorded from the 5 areas designated in Fig. 2. ERGs of a WT and a Tg rabbit at 3 months are shown. The focal rod ERGs of the Tg rabbit were non-recordable at 3 months.

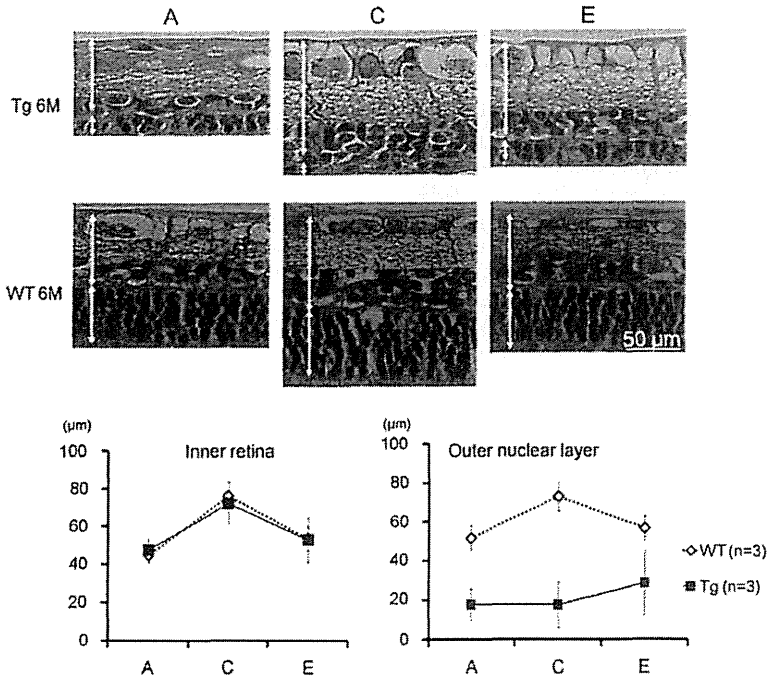

Fig. 6. Retinal histology of Tg rabbits. Vertical retinal sections from 4 mm superior to the optic nerve head (A), 2 mm (C) and 6 mm (E) inferior to the optic nerve head of 6-months-old WT and Tg rabbits are shown in the upper half. White two way arrows in the micrograph indicate thickness of inner retina and outer nuclear layer (ONL) respectively. Thickness of the inner retina and ONL along the vertical meridian measured at 3 retinal locations are shown in the lower. Mean ± SD of 3 WT and 3 Tg rabbits are plotted.

4. Discussion

We recorded focal ERGs from 5 retinal areas of Tg rabbits during the course of retinal degeneration. Our previous study indicated the Tg rabbits had a progressive dysfunction of the rods (Kondo et al., 2009). Because focal ERGs recorded under scotopic conditions are non-recordable at 3 months, we were not able to evaluate local rod function in Tg rabbit. The amplitudes of the focal cone ERG b-waves became progressively smaller with increasing age in all regions, and there were no differences in the amplitudes from the 5 areas. On the other hand, the amplitudes of the summed OPs had regional variations with that of the superior retina (area A) significantly larger than that from other areas at both 3 and 6 months.

4.1. Focal ERGs from WT rabbits

The characteristics of the multifocal ERGs (mfERGs) of normal rabbits or Tg rabbits have been determined (Horiguchi et al., 1998; Wallenten, Andreasson, & Ghosh, 2008; Yokoyama et al., 2010). However to the best of our knowledge, this is the first report of focal ERGs recorded from Tg rabbits. The waveforms of mfERGs are derived from mathematical modeling of the potential changes of the retinal neurons (Sutter & Tran, 1992), while the waveforms of focal ERGs are the potential changes of the retinal neurons. Our laboratory has studied focal ERGs of humans and monkeys using this technique for more than twenty years (Miyake, 1990; Miyake et al., 1989; Shiroyama & Miyake, 1990). Monitoring the fundus during the recording was essential because the animals cannot fixate a target, and thus we believe that our system is a more appropriate method of recording ERGs from localized areas than mfERGs.

The focal cone ERGs of rabbits at light on consisted of a- and b-waves with OPs as in primates (Kondo et al., 2008; Miyake et al., 1989). When the light is turned off, a d-wave appeared in the primate ERGs but was barely detected in rabbits. The amplitude of the focal cone ERGs from the fovea in human is about 5 μV, while that from the visual streak of rabbits was about 3 μV. This lower amplitude may be because the cone density is higher in humans. Comparing the five retinal areas, the b-wave amplitudes from the visual streak (B–D) was larger than that of two other areas (A and E). These results are comparable to histological data that show that the cone density is highest in the visual streak (Famiglietti & Sharpe, 1995; Juliusson et al., 1994). For the focal rod ERGs of WT rabbits, the waveforms and amplitudes were not different among the different retinal areas. In addition, the waveforms were similar to those of the full-field rod responses elicited with weak stimuli under dark-adapted conditions (Marmor et al., 2009). These results indicate that the rod function is not significantly different in the regions tested.

4.2. Focal ERGs from Tg rabbits

We followed the changes in the amplitudes of the focal cone ERGs during the course of retinal degeneration in Tg rabbit. Earlier studies reported that reductions in the mfERG amplitudes of mice, cats, pigs, and rabbits with genetically-induced retinal degeneration (Ng et al., 2008; Seeliger & Narfstrom, 2000; Seeliger et al., 2003; Yokoyama et al., 2010). However, the OPs of the mfERGs could not be analyzed. Because the OPs originate mainly from the inner retina, it is reasonable to analyze the OPs to determine whether functional changes of the inner retinal neurons are present in Tg rabbits.

Earlier, we reported that the thickness of the outer nuclear layer in the visual streak of albino Tg rabbits was one-half of that of WT at 3 months and one-third of that of WT rabbits at 6 months (Kondo et al., 2009). These results are comparable with our focal cone ERG results; the amplitude of the b-waves of the focal cone ERGs was one-third of WT rabbit at 3 months, one-fourth of that at 6 months, and non-recordable at 12 months. We also reported that the loss of photoreceptors in the visual streak was more severe than that at 6 mm superior to the optic nerve head (ONH) and 8 mm inferior to the ONH. However, we did not find distinct regional differences in the amplitudes of the b-waves of the focal cone

ERGs probably because the amplitude of the focal ERGs was small and the signal-to-noise ratio was too large to detect the differences. Our focal cone ERGs might be less sensitive in detecting regional differences than histopathological analyses.

We have reported the change of the full-field cone ERGs in Tg rabbit in earlier studies (Hirota et al., 2012; Kondo et al., 2008; Sakai et al., 2009). However, the focal ERGs results contradict our earlier findings that there was no significant difference in the amplitude of the full-field cone b-wave V_{max} between Tg and Wt rabbits even at 12 months (see Fig. 3 and Table 1 in Sakai et al., 2009). We also reported that the half-saturation coefficient (K) was already reduced significantly at 3 months (Sakai et al., 2009). These findings suggest that dimmer flashes can detect the differences between Tg and WT rabbits more easily. In addition, slight degeneration of the photoreceptors would not affect coneERG b-wave amplitudes elicited by high intensity stimuli because the b-wave amplitudes are at the saturated level. Our focal cone ERGs were recorded with relatively dim stimulus (30 cd/m^2) to avoid stray light effects and our system seemed to be more suitable for detecting functional loss due to photoreceptor degeneration.

An interesting finding in this study was that the amplitudes of the OPs were better preserved than the b-waves and the OPs/b-wave ratio was greater than that in WT rabbits at every recording area at 3 months. In addition, the sum of the OPs at area A was best preserved, and the sum was significantly larger than that of other areas. We have reported that the OPs of the full-field cone ERGs of 3-month-old Tg rabbit were 1.7 times larger than that of WT rabbits (Sakai et al., 2009). We suggest that secondary functional changes in the inner retinal neurons, retinal ganglion cells, and/or amacrine cells, caused this phenomenon because these OPs were TTX sensitive (Sakai et al., 2009). Although the amplitudes of the OPs were not supernormal even at area A, our results suggest there are regional differences in secondary functional alterations in the inner retinal neurons after photoreceptor death. When we compared the histology of the dorsal, visual streak, and ventral retina from 6-months-old rabbit in hematoxylin and eosin stained sections, we were not able to find differences in the thickness of the inner retina. A previous OCT study showed that the inner nuclear layer (INL) thickness in RP rabbits did not differ from that of WT rabbits (Muraoka et al., 2012). To explore the mechanisms of large OPs at ventral site, we will need to evaluate the regional differences of the inner retinal histopathology more precisely in the future.

We reported that the OPs of the focal macular ERGs of RP patients were better preserved than the a- and b-waves (Ikenoya et al., 2007). These data raise the possibility that similar secondary functional changes can occur in some RP patients.

Finally, we believe that this Tg rabbit will serve as a useful mid-sized animal model with which to develop treatments including cell transplantation (MacLaren et al., 2006) and retinal prosthesis (Nishida et al., 2010; Weiland, Liu, & Humayun, 2005).

Acknowledgments

We thank Prof. Duco I. Hamasaki for editing the manuscript.

Grant Support: 20592075 (M.K.) and 25462709 (S.U.) from the Ministry of Education, Science, Sports and Culture, Japan.

References

Chan, H. L., & Brown, B. (1998). Investigation of retinitis pigmentosa using the multifocal electroretinogram. *Ophthalmic and Physiological Optics, 18*(4), 335–350.

Dong, C. J., Agey, P., & Hare, W. A. (2004). Origins of the electroretinogram oscillatory potentials in the rabbit retina. *Visual Neuroscience, 21*(4), 533–543.

Famiglietti, E. V., & Sharpe, S. J. (1995). Regional topography of rod and immunocytochemically characterized "blue" and "green" cone photoreceptors in rabbit retina. *Visual Neuroscience, 12*(6), 1151–1175.

Heckenlively, J. R. (1988). *Retinitis pigmentosa*. JB Lippincott, Philadelphia (pp. 221–252).

Hirota, R., Kondo, M., Ueno, S., Sakai, T., Koyasu, T., & Terasaki, H. (2012). Photoreceptor and post-photoreceptoral contributions to photopic ERG a-wave in rhodopsin P347L transgenic rabbits. *Investigative Ophthalmol and Visual Science, 53*(3), 1467–1472.

Hood, D. C., Holopigian, K., Greenstein, V., Seiple, W., Li, J., Sutter, E. E., et al. (1998). Assessment of local retinal function in patients with retinitis pigmentosa using the multi-focal ERG technique. *Vision Research, 38*(1), 163–179.

Horiguchi, M., Suzuki, S., Kondo, M., Tanikawa, A., & Miyake, Y. (1998). Effect of glutamate analogues and inhibitory neurotransmitters on the electroretinograms elicited by random sequence stimuli in rabbits. *Investigative Ophthalmology & Visual Science, 39*(11), 2171–2176.

Ikenoya, K., Kondo, M., Piao, C. H., Kachi, S., Miyake, Y., & Terasaki, H. (2007). Preservation of macular oscillatory potentials in eyes of patients with retinitis pigmentosa and normal visual acuity. *Investigative Ophthalmology & Visual Science, 48*(7), 3312–3317.

Juliusson, B., Bergstrom, A., Rohlich, P., Ehinger, B., van Veen, T., & Szel, A. (1994). Complementary cone fields of the rabbit retina. *Investigative Ophthalmology & Visual Science, 35*(3), 811–818.

Kondo, M., Sakai, T., Komeima, K., Kurimoto, Y., Ueno, S., Nishizawa, Y., et al. (2009). Generation of a transgenic rabbit model of retinal degeneration. *Investigative Ophthalmology & Visual Science, 50*(3), 1371–1377.

Kondo, M., Ueno, S., Piao, C. H., Miyake, Y., & Terasaki, H. (2008). Comparison of focal macular cone ERGs in complete-type congenital stationary night blindness and APB-treated monkeys. *Vision Research, 48*(2), 273–280.

MacLaren, R. E., Pearson, R. A., MacNeil, A., Douglas, R. H., Salt, T. E., Akimoto, M., et al. (2006). Retinal repair by transplantation of photoreceptor precursors. *Nature, 444*(7116), 203–207.

Marc, R. E., Jones, B. W., Anderson, J. R., Kinard, K., Marshak, D. W., Wilson, J. H., et al. (2007). Neural reprogramming in retinal degeneration. *Investigative Ophthalmology & Visual Science, 48*(7), 3364–3371.

Marmor, M. F., Fulton, A. B., Holder, G. E., Miyake, Y., Brigell, M., & Bach, M. (2009). ISCEV Standard for full-field clinical electroretinography (2008 update). *Documenta Ophthalmologica, 118*(1), 69–77.

Miyake, Y. (1990). Macular oscillatory potentials in humans. Macular OPs. *Documenta Ophthalmologica, 75*(2), 111–124.

Miyake, Y., Shiroyama, N., Horiguchi, M., & Ota, I. (1989). Asymmetry of focal ERG in human macular region. *Investigative Ophthalmology & Visual Science, 30*(8), 1743–1749.

Muraoka, Y., Ikeda, H. O., Nakano, N., Hangai, M., Toda, Y., Okamoto-Furuta, K., et al. (2012). Real-time imaging of rabbit retina with retinal degeneration by using spectral-domain optical coherence tomography. *PLoS One, 7*(4), e36135.

Ng, Y. F., Chan, H. H., Chu, P. H., To, C. H., Gilger, B. C., Petters, R. M., et al. (2008). Multifocal electroretinogram in rhodopsin P347L transgenic pigs. *Investigative Ophthalmology & Visual Science, 49*(5), 2208–2215.

Nishida, K., Kamei, M., Kondo, M., Sakaguchi, H., Suzuki, M., Fujikado, T., et al. (2010). Efficacy of suprachoroidal–transretinal stimulation in a rabbit model of retinal degeneration. *Investigative Ophthalmology & Visual Science, 51*(4), 2263–2268.

Sakai, T., Kondo, M., Ueno, S., Koyasu, T., Komeima, K., & Terasaki, H. (2009). Supernormal ERG oscillatory potentials in transgenic rabbit with rhodopsin P347L mutation and retinal degeneration. *Investigative Ophthalmology and Visual Science, 50*(9), 4402–4409.

Seeliger, M. W., Kretschmann, U. H., Apfelstedt-Sylla, E., & Zrenner, E. (1998). Implicit time topography of multifocal electroretinograms. *Investigative Ophthalmology & Visual Science, 39*(5), 718–723.

Seeliger, M. W., & Narfstrom, K. (2000). Functional assessment of the regional distribution of disease in a cat model of hereditary retinal degeneration. *Investigative Ophthalmology & Visual Science, 41*(7), 1998–2005.

Seeliger, M. W., Weber, B. H., Besch, D., Zrenner, E., Schrewe, H., & Mayser, H. (2003). MfERG waveform characteristics in the RS1h mouse model featuring a 'negative' ERG. *Documenta Ophthalmologica, 107*(1), 37–44.

Shiroyama, N., & Miyake, Y. (1990). Analysis of focal macular ERG in idiopathic central serous chorioretinopathy. *Nippon Ganka Gakkai Zasshi, 94*(11), 1048–1056.

Sugita, T., Kondo, M., Piao, C. H., Ito, Y., & Terasaki, H. (2008). Correlation between macular volume and focal macular electroretinogram in patients with retinitis pigmentosa. *Investigative Ophthalmology & Visual Science, 49*(8), 3551–3558.

Sutter, E. E., & Tran, D. (1992). The field topography of ERG components in man – I. The photopic luminance response. *Vision Research, 32*(3), 433–446.

Vajaranant, T. S., Seiple, W., Szlyk, J. P., & Fishman, G. A. (2002). Detection using the multifocal electroretinogram of mosaic retinal dysfunction in carriers of X-linked retinitis pigmentosa. *Ophthalmology, 109*(3), 560–568.

Wachtmeister, L. (1998). Oscillatory potentials in the retina: What do they reveal. *Progress in Retinal and Eye Research, 17*(4), 485–521.

Wallenten, K. G., Andreasson, S., & Ghosh, F. (2008). Retinal function after vitrectomy. *Retina, 28*(4), 558–563.

Weiland, J. D., Liu, W., & Humayun, M. S. (2005). Retinal prosthesis. *Annual Review of Biomedical Engineering, 7*, 361–401.

Weleber, R. G., and Gregory-Evance, K., (2006). *Retinitis pigmentosa and allied disorders* (4th ed.). Retina 1 (Mosby St. Louis. Basic Science and Inherited Retinal Disease).

Yokoyama, D., Machida, S., Kondo, M., Terasaki, H., Nishimura, T., & Kurosaka, D. (2010). Pharmacological dissection of multifocal electroretinograms of rabbits with Pro347Leu rhodopsin mutation. *Japanese Journal of Ophthalmology, 54*(5), 458–466.

Eye (2013) 27, 871–877

www.nature.com/eye

CLINICAL STUDY

Displacement of foveal area toward optic disc after macular hole surgery with internal limiting membrane peeling

K Kawano[1], Y Ito[1], M Kondo[1,2], K Ishikawa[1], S Kachi[1], S Ueno[1], Y Iguchi[1] and H Terasaki[1]

Abstract

Purpose To determine whether there is a displacement of the fovea toward the optic disc after successful macular hole (MH) surgery with internal limiting membrane (ILM) peeling.

Methods The medical records of 54 eyes of 53 patients that had undergone pars plana vitrectomy with ILM peeling and gas or air tamponade for an idiopathic MH were evaluated. Spectral-domain optical coherence tomography (OCT) had been performed before and >6 months after the surgery. The preoperative distances between the center of the MH and the optic disc (MH-OD), center of the MH and the bifurcation or crossing of retinal vessels (MH-RV) were measured in the OCT images. In addition, the postoperative distance between the center of the fovea and optic disc (F-OD) and the center of the fovea and the same bifurcation or crossing of retinal vessels (F-RV) were measured in the OCT images.

Results The F-OD was 2.67 ± 0.33 disc diameters (DD), which was significantly shorter than that of the MH-OD of 2.77 ± 0.33 DD ($P<0.001$). The F-RV was also significantly shorter than the MH-RV on the inner nasal area (from 0.85 ± 0.16DD to 0.79 ± 0.15DD; $P<0.001$), the inner temporal area (from 0.82 ± 0.15DD to 0.77 ± 0.14DD; $P<0.001$), and outer nasal area (from 1.70 ± 0.31DD to 1.65 ± 0.32DD; $P<0.001$), but it was significantly longer than the MH-RV in the outer temporal area (from 1.65 ± 0.29DD to 1.68 ± 0.29DD; $P<0.001$).

Conclusion Our results showed that successful closure of a MH by vitrectomy with ILM peeling and gas tamponade leads to a displacement of the center of the macula toward the optic disc.

Eye (2013) 27, 871–877; doi:10.1038/eye.2013.99; published online 24 May 2013

Keywords: macular hole; vitrectomy; internal limiting membrane peeling; displacement of fovea

Introduction

An idiopathic macular hole (MH) can be successfully closed by vitrectomy,[1–6] and the success rate is improved if the internal limiting membrane (ILM) is peeled during the vitrectomy.[2–6] Although the mechanism causing the MH has been essentially determined,[7–12] the mechanism for the MH closure has not been definitively determined.

Yanagita *et al*[13] reported that after a closure of a MH by vitrectomy, the retinal blood vessels near the MH are displaced toward the center of the fovea in all cases. They suggested that the retina around the MH moved toward the foveal pit after vitrectomy. On the other hand, we have noted that in many cases the retinal vessels in the macular area appeared to move toward the optic disc after vitrectomy that successfully closed a MH.

Thus, the purpose of this study was to test the hypothesis that the center of the macular area moves nasally toward the optic disc after successful closure of a MH by vitrectomy with ILM peeling.

[1]Department of Ophthalmology, Nagoya University School of Medicine, Nagoya, Japan

[2]Department of Ophthalmology, Mie University School of Medicine, Tsu, Japan

Correspondence:
Y Ito, Department of Ophthalmology, Nagoya University School of Medicine, 65 Tsuruma-cho, Showa-ku, Nagoya, Aichi 466-8550, Japan.
Tel: +81 5 2744 2271;
Fax: +81 5 2744 2279.
E-mail: yasu@med.nagoya-u.ac.jp

Received: 17 December 2012
Accepted in revised form: 23 April 2013
Published online: 24 May 2013

Meeting Presentation: Parts of this study were presented at the Japanese Clinical Ophthalmological Society Meeting, October 2011, and the Japanese Ophthalmological Society Meeting, May 2012.

Materials and methods

Study population

We reviewed the medical charts of 54 eyes of 53 patients who underwent successful vitrectomy for an idiopathic MH at the Nagoya University Hospital between October 2008 and May 2012. There were 33 women and 20 men. The mean ± SD of the age was 65.3 ± 6.0 years with a range of 54–78 years. There were 25 stage-2 MHs (46%), 12 stage-3 MHs (22%), and 17 stage-4 MHs (31%).[7] All MHs were closed after a single surgery.

Eyes excluded from the statistical analyses were those with a reopening of the MH, with high myopia, or with a retinal detachment combined with the MH. Eyes with other macular diseases, such as age-related macular degeneration, were also excluded.

We also reviewed the charts of five eyes of five patients who had an idiopathic MH that closed spontaneously. The measurements made on these five eyes were identical to that of eyes that underwent vitrectomy.

The protocol for this study was approved by the institutional review board of the Nagoya University School of Medicine, and the procedures used conformed to the tenets of the Declaration of Helsinki.

Surgical techniques

A three-port pars plana vitrectomy with ILM peeling was carried out with 23- or 25-gauge instruments in all cases. All of the patients underwent combined cataract surgery except one patient who was pseudophakic. Triamcinolone acetonide was used for staining the ILM in all 54 eyes. The area of ILM peeling was symmetrical around the fovea and was about four disc diameters (DD). Sulfur hexafluoride (0.5–1.0 ml) gas was used in 38 eyes, perfluoropropane (0.5–0.8 ml) gas in 15 eyes, and simple fluid gas exchange without any gas injection was used in one eye as a tamponade. The patients were instructed to maintain a face-down position as much as possible until the closure of MHs was confirmed by OCT.

Examination and measurement procedures

All patients underwent a complete ophthalmic examination, including measurements of the best-corrected visual acuity (BCVA), slit-lamp biomicroscopy, fundus examination, and optical coherence tomography (OCT; Cirrus OCT; Carl Zeiss Meditec, Dublin, CA, USA) before and 1–2 weeks, 1–3 months, and >6 months after the vitrectomy. Axial length was measured in all eyes preoperatively (IOL master, Carl Zeiss Meditec). The fovea was scanned with the 200 × 200 Macular Cube protocol of the Cirrus HD-OCT. OCT images were excluded if the eye moved during the scans.

The distance across the fundus was measured in the Cirrus OCT images.[14] The Cirrus OCT instrument allows a direct registration of the OCT projection maps onto the infrared line scanning ophthalmoscopic image. The location of the center of the MH or postoperative foveola was determined by realigning the vertical and horizontal OCT scans in the analysis window manually (Figures 1a, b, d and e). In cases where the postoperative foveal pit was irregular, center of fovea was considered to be the thinnest part in the OCT image. In cases where the postoperative foveal pit was flat, the center of the fovea was considered to be the center of foveal pit.

The preoperative distance between center of MH and optic disc (MH-OD) and the distance between center of the MH and a bifurcation or crossing of retina vessels (MH-RV) were measured in the Cirrus OCT images (Figure 1c). In the same way, the postoperative distance between the fovea and optic disc (F-OD), and the distance between the fovea and a bifurcation or crossing of retina vessels (F-RV) were measured in the Cirrus OCT images. Each distance was measured manually with the caliper function embedded in the OCT instrument. To compensate for variations in the magnification of each scan, each distance was divided by vertical diameter of the optic disc, and the distance was expressed in DD units.

The locations of the bifurcation or crossing of the retinal vessels were selected in four areas: the inner nasal area, the inner temporal area, the outer nasal area, and the outer temporal area (Figure 1c). The inner areas were within a circle of two DD centered on the fovea, and the outer area was between circles of two and four DDs centered on fovea. The margin between the nasal and temporal areas was a vertical line passing through the fovea. The movement of the macula in each area was analyzed separately.

Eyes with spontaneous closure of MH

The MHs of five eyes closed spontaneously, and both the pre-closure and post-closure OCT images were available. The measurements of the displacement were done identically to the eyes that underwent vitrectomy. The mean ± SD age of these three women and two men was 65.6 ± 6.7 years with a range of 56–73 years. There were two stage-2 MHs (40%) and three stage-3 MHs (60%).

Statistical analyses

The significance of the differences between the pre- and postoperative values was determined by paired *t*-tests, and single and stepwise regression analysis was used to determine the parameters that were significantly associated with the distance of movement of the fovea (PASW statistics version 18.0; SPSS Inc and IBM

Company, Chicago, IL, USA). A $P<0.05$ was taken to be statistically significant.

Results

The pre- and postoperative OCT images of 36 eyes of 36 patients at 1–3 months and >6 months were of sufficient quality to be analyzed. The mean ± SD preoperative MH-OD distance was 2.77 ± 0.33 DD with a range of 2.08–3.47 DD. The mean postoperative F-OD distance was 2.67 ± 0.32 DD with a range of 2.05–3.34 DD at 1–3 months, and 2.67 ± 0.33 DD with a range of 2.03–3.37 DD at >6 months. The F-OD distance at 1–3 and >6 months after surgery were significantly shorter than the MH-OD by 3.3 ± 2.0% and 3.6% ± 1.8%, respectively, (both $P<0.001$, paired *t*-tests).

The OCT images of 13 eyes that were recorded within 2 weeks after surgery and were good enough to be analyzed were available. In these 13 eyes, the average MH-OD distance was 2.61 ± 0.16 DD, and the F-OD distance was 2.57 ± 0.18 DD at 1–2 weeks, 2.54 ± 0.16 DD at 1–3 months, and 2.53 ± 0.16 DD at >6 months after the vitrectomy. The F-OD distance at 1–2 weeks, 1–3 months, and >6 months after surgery were significantly shorter than the MH-OD distance by 1.8% ± 1.5% ($P=0.001$, paired *t*-test), by 2.9 ± 1.4% ($P<0.001$, paired *t*-test), and by 3.1% ± 1.5% ($P<0.001$, paired *t*-test; Figure 2a).

The mean ± SD of the MH-RV distance in the inner nasal area for the 36 eyes was 0.85 ± 0.16 DD preoperatively. The mean ± SD of the F-RV distance in the inner nasal area was 0.80 ± 0.16 DD at 1–3 months after surgery and 0.79 ± 0.15 DD at >6 months after the vitrectomy. The F-RV distance in the inner nasal area were significantly shorter than the MH-RV distance by 6.6 ± 4.4% ($P<0.001$, paired *t*-test) at 1–3 months and by 7.2% ± 4.1% ($P<0.001$, paired *t*-test) at 6 months after the vitrectomy (Figure 3).

The mean ± SD of the MH-RV distance in the inner temporal area was 0.82 ± 0.15 DD preoperatively. The mean of the F-RV distance in the inner temporal area was 0.77 ± 0.15 DD at 1–3 months after surgery and 0.77 ± 0.14 DD at >6 months after the vitrectomy. The F-RV distance

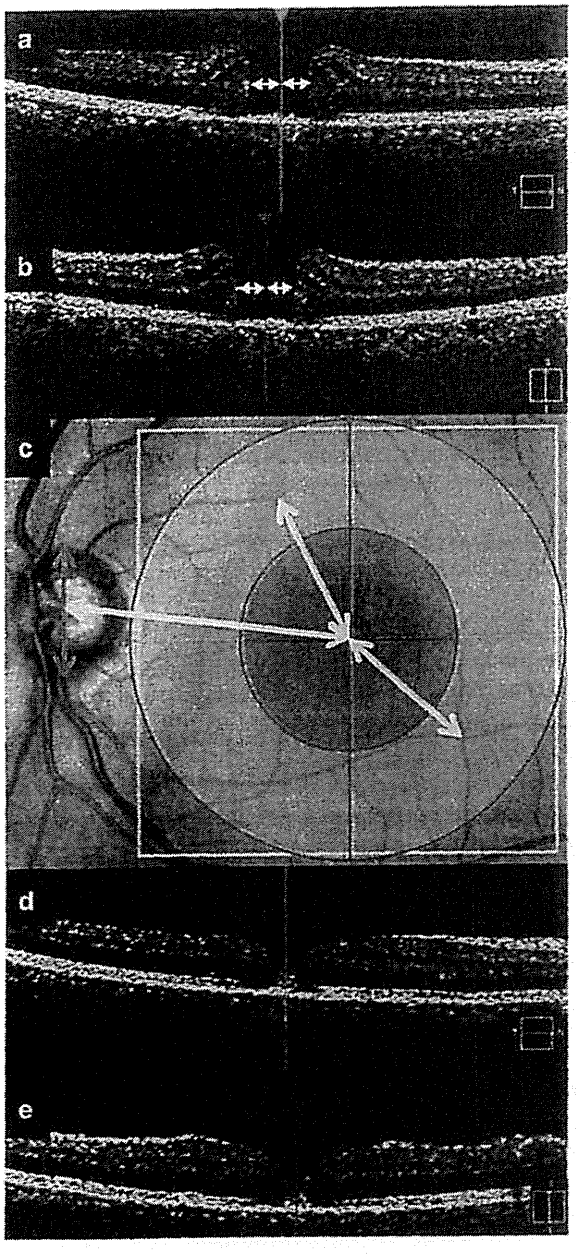

Figure 1 Diagrams of how the distances between center of MH or postoperative fovea and major landmarks are measured in the OCT images and infrared line scanning ophthalmoscope images. (a, b) Preoperative OCT images. (a) is an image obtained by a horizontal scan and (b) is a vertical scan in the raster map program of Cirrus OCT. Pink line in (a) indicates the location of the vertical scan (b). Blue line in (b) indicates the location of the horizontal scan (a). Center of MH can be easily identified by moving the location of scans (blue and pink lines) to the center of MH (white arrowheads). (c) Distance between the center of the macular hole and optic disc or bifurcation or crossing of retinal vessels were measured manually using the caliper function of the Cirrus OCT (yellow arrows). Vertical diameter of the optic disc was also measured similarly (blue arrow). The location of a bifurcation or crossing of retinal vessels were made in four areas of the macular area; inner nasal, inner temporal, outer nasal, and outer temporal area. The diameter of the ring is two and four DD (red circles). The vertical line running through fovea divided the retina into nasal and temporal halves (red vertical line). (d, e) Postoperative OCT images. (d) is an image obtained by a horizontal scan and (b) is a vertical scan in the raster map program of Cirrus OCT. Pink line in (d) indicates the location of the vertical scan (e). Blue line in (e) indicates the location of the horizontal scan (d). Center of fovea can be easily identified by moving the location of scans (blue and pink lines) to the center of fovea.

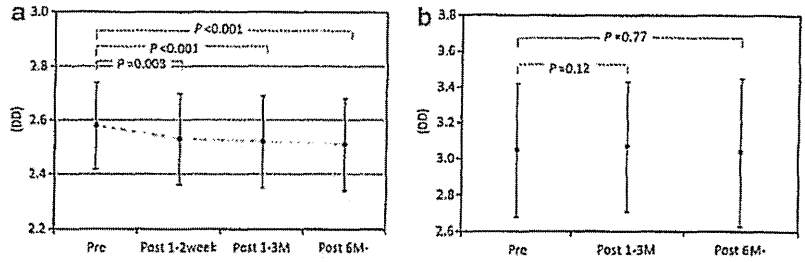

Figure 2 Graphs showing the degree of foveal movement toward optic disc. (a) Changes in the distance between the fovea and optic disc in eyes that had undergone surgery. The preoperative distance was between center of macular hole and optic disc. Postoperative distance was between fovea and optic disc. Macular retina moved significantly toward the optic disc after surgery. (b) Changes in the distance between the fovea and optic disc in eyes with a spontaneous closure. Distance was not significantly different, indicating that the macular retina did not move after the closure.

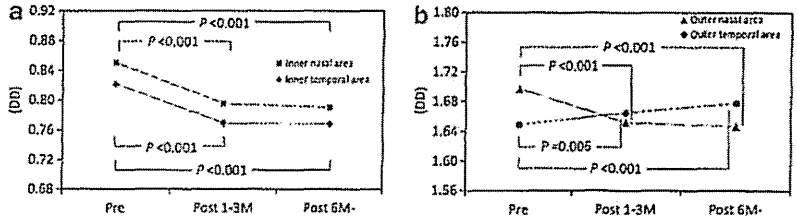

Figure 3 Graphs showing the degree of movement of the macular retina. (a) Changes in the distance between the fovea and bifurcation or crossing of retinal vessels in the inner ring. Macular retina in inner ring moved significantly toward the fovea after surgery. (b) Changes in the distance between the fovea and bifurcation or crossing in the outer ring. The distance to the nasal outer areas decreased significantly after surgery. In contrast, the distance to the temporal outer area increased significantly after surgery. This is probably because fovea moved toward optic disc.

in the inner temporal area was significantly shorter than the MH-RV by 6.5 ± 4.5% ($P<0.001$, paired t-test) at 1–3 months after surgery and by 6.5% ± 4.4% ($P<0.001$, paired t-test) at >6 months after surgery.

The mean ± SD MH-RV distance in the outer nasal area was 1.70 ± 0.31 DD preoperatively. The mean ± SD F-RV distance in the outer nasal area was 1.65 ± 0.31 DD at 1–3 months after surgery and 1.65 ± 0.32 DD at >6 months after the vitrectomy. The R-RV distance in the outer nasal area were significantly shorter than the MH-RV distance by 2.8 ± 2.9% ($P<0.001$, paired t-test) at 1–3 months and by 3.1 ± 3.3% ($P<0.001$, paired t-test) at >6 months after the vitrectomy.

The mean ± SD MH-RV distance in the outer temporal area was 1.65 ± 0.29 DD preoperatively. The mean ± SD F-RV distance in the outer temporal area was 1.67 ± 0.29 DD at 1–3 months and 1.68 ± 0.29 DD at >6 months after the vitrectomy. The F-RV in the outer temporal area was significantly longer than the MH-RV by 1.0 ± 2.8% ($P=0.006$, paired t-test) at 1–3 months and by 1.8 ± 3.0% ($P<0.001$, paired t-test) at >6 months after the vitrectomy.

The mean ± SD diameter of the MHs was 693 ± 318 μm with a range of 234–1778 μm or 0.42 ± 0.20 DD with a range of 0.13–1.08 DD. The difference between the preoperative MH-OD and postoperative F-OD, that is, the movement of the fovea at >6 months after the vitrectomy, was greater than the radius of the MH in eight eyes (22.2%).

The mean BCVA was 0.68 ± 0.23 logMAR units with a range of 0.3–1.2 logMAR units preoperatively and 0.29 ± 0.24 logMAR units with a range of 0.0–1.0 logMAR units postoperatively.

Single and stepwise regression analysis showed that the diameter of the MHs, preoperative and postoperative BCVAs, improvements in the BCVA, age and axial length were not significantly associated with the difference between the MH-OD and F-OD distances (Table 1).

A representative case is shown in Figure 4. When the pre- and postoperative fundus images were overlapped, the movement of the retinal vessels in the center of macular area toward the optic disc could be clearly seen.

Eyes with spontaneous closure

The mean ± SD of the MH-OD distance while the MH was open was 3.05 ± 0.37 DD, with a range of 2.71–3.64 DD. The mean ± SD of the F-OD distance after a spontaneous closure of the MH was 3.04 ± 0.41 DD, with a range of 2.69–3.70 DD at >6 months after the spontaneous closure (Figure 2b). The difference in the MH-OD and F-OD distances were not significant. The MH-RV and F-RV in the inner nasal area were 0.80 ± 0.09 DD with a range of 0.66–0.90 DD and 0.81 ± 0.10 DD with

Table 1 Results of simple regression analysis to find the parameters re-rated with the movement distances

	R^2	P
Diameter of the macular holes	0.001	0.83
Preoperative BCVAs	0.013	0.42
Postoperative BCVAs	0.005	0.59
Improvements in the BCVAs	0.002	0.75
Age	0.007	0.54
Axial length	0.008	0.53

Abbreviation: BCVA, best-corrected visual acuity.

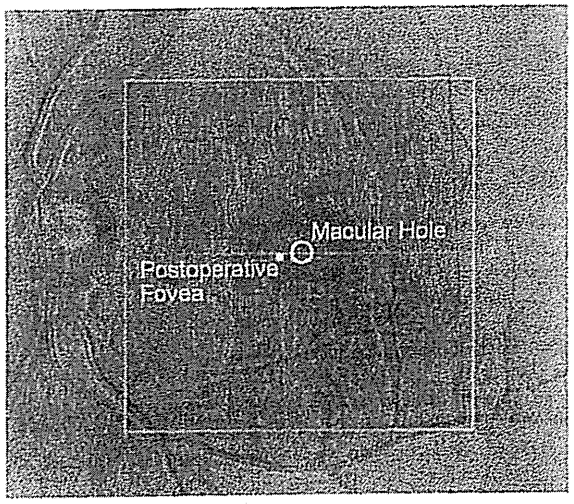

Figure 4 Representative case with a stage-2 MH in a 55-year-old man. This is a composite OCT image that was made by overlapping preoperative and postoperative images after changing to the gray scale. The black retinal vessels are the preoperative location of the retinal vessels, and white vessels are postoperative location. White ring shows the MH. White dot shows postoperative fovea. This image clearly shows that the macular retina has moved toward the optic disc.

a range from 0.65 to −0.91 DD, respectively. MH-RV and F-RV distances in the inner temporal area were 0.72 ± 0.10 DD with a range of 0.59–0.85 DD and 0.71 ± 0.10 DD with a range of 0.58–0.84 DD, respectively. The MH-RV and F-RV distances in the outer nasal area were 1.72 ± 0.17 DD with a range of 1.50–1.97 DD and 1.72 ± 0.16 DD with a range of 1.52–0.96 DD, respectively. The MH-RV and F-RV distances in the outer temporal area were 1.63 ± 0.23 DD with a range of 1.31–1.91 DD and 1.62 ± 0.24 DD with a range of 1.31–1.93 DD, respectively. The differences in the MH-RV and F-RV distances were not significant in all four areas.

Discussion

Our results showed that the F-OD distance was significantly shorter than the MH-OD distance. This indicates that the center of the macular area moved toward the optic disc after vitrectomy with ILM peeling. There is a possibility that the MH closure caused this displacement. However, the MH-OD and F-OD distances were not different in eyes with a spontaneous closure of the MH. Therefore, the ILM peeling was most likely the cause of this movement. Under natural conditions, the traction of the ILM on the fovea from the temporal side may be stronger than that from nasal side because there is no ILM on the optic disc. We suggest that once the ILM is peeled, the balance may be altered, and the fovea is then displaced toward the optic disc. Further studies are needed to determine whether ILM peeling can cause the macular movement in other diseases after surgery with ILM peeling. A study analyzing eyes with diabetic macular edema treated by vitrectomy with ILM peeling is ongoing in our clinic.

There is a possibility that the MH may close asymmetrically around the center of the MH. However, the movement in eight eyes was larger than the radius of the MH. Therefore, the fovea most likely moved toward the optic disc after the surgery. This displacement of foveal area toward optic disc could be clearly seen in the images made by overlapping pre- and postoperative fundus images (Figure 4).

The average F-RV distance of the inner nasal and temporal area was significantly shorter than that of the MH-RV. This indicates that the retina around the MH moved toward the center of the MH after the MH was closed. In contrast, the F-RV distance in the outer temporal area was significantly greater than the MH-RF distance. The movement of the fovea toward the optic disc may cause this expansion.

A movement of the macular area was reported in eyes with an epiretinal membrane,[14] in eyes after the removal of an epiretinal membrane,[15] and in eyes after retinal detachment surgery.[16] Macular translocation surgeries for myopic choroidal neovascularization and age-related macular degeneration have also been intentionally moved from the foveal area to other locations.[17–24] Thus, the macular retina is movable depending on the circumstances and can function on any retinal pigment epithelium.

Our single and stepwise regression analysis showed that the pre- and postoperative BCVAs and the improvements in the BCVA were not significantly associated with the degree of retinal movement. A significant relationship between the change in the position of the macular area and functional changes was not found in this study. In eyes with an epiretinal membrane, the extent of tractional foveal dystopia was found to be correlated with a decrease of the visual acuity.[14] Further studies are needed to determine the relationship between the degree of displacement and any functional changes of the retina.

The nasal movement of the fovea may cause a pseudoesotropia. As we did not evaluate the eye position, we cannot state whether a change of eye position occurred. However, none of the patients complained of diplopia postoperatively, and none had an obvious pseudoesotropia. As the average distance of movements was 0.09 DD or about 0.4 degree or 0.7 prism diopters, it may be difficult to detect. Further studies are needed to determine whether changes in the eye position occurred postoperatively.

One of the limitations in this study is that cataract surgery may cause the change of the distance in the OCT image. However, we measured the distance with DD unit. Therefore, even if this change occurs, this change is compensated and the distance in the OCT image before and after the surgery can be compared.

In conclusion, we have shown that center of the macula is displaced toward the optic disc after vitrectomy for MH with ILM peeling. As all of the MHs were closed after the initial surgery, it is not known whether this movement contributes to the success of the surgery. Further studies are needed to investigate this phenomenon.

Summary

What was known before

- An idiopathic MH can be successfully closed by vitrectomy, and the success rate is improved if the ILM is peeled during the vitrectomy.
- However, the mechanism for the MH closure has not been definitively determined.

What this study adds

- Our results showed that successful closure of a MH by vitrectomy with ILM peeling and gas tamponade results in a displacement of the center of the macula toward the optic disc.

Conflict of interest

The authors declare no conflict of interest.

Acknowledgements

This study was supported by the Grant-in Aid for Scientific Research from the Ministry of Education, Culture, Sports, Science, and Technology of Japan (Dr Ito, C2159225).

References

1 Kelly NE, Wendel RT. Vitreous surgery for idiopathic macular holes: results of a pilot study. *Arch Ophthalmol* 1991; 109: 654–659.
2 Park DW, Sipperley JO, Sneed SR, Dugel PU, Jacobsen J. Macular hole surgery with internal-limiting membrane peeling and intravitreous air. *Ophthalmology* 1999; 106: 1392–1398.
3 Brooks Jr, HL. Macular hole surgery with and without internal limiting membrane peeling. *Ophthalmology* 2000; 107: 1939–1949.
4 Kumagai K, Furukawa M, Ogino N, Uemura A, Demizu S, Larson E. Vitreous surgery with and without internal limiting membrane peeling for macular hole repair. *Retina* 2004; 24: 721–727.
5 Kadonosono K, Itoh N, Uchio E, Nakamura S, Ohno S. Staining of internal limiting membrane in macular hole surgery. *Arch Ophthalmol* 2000; 118: 1116–1118.
6 Enaida H, Hisatomi T, Hata Y, Ueno A, Goto Y, Yamada T *et al*. Brilliant blue G selectively stains the internal limiting membrane/brilliant blue G-assisted membrane peeling. *Retina* 2006; 26: 631–636.
7 Gass JD. Idiopathic senile macular hole. Its early stages and pathogenesis. *Arch Ophthalmol* 1988; 106: 629–639.
8 Gass JD. Reappraisal of biomicroscopic classification of stages of development of a macular hole. *Am J Ophthalmol* 1995; 119: 752–759.
9 Gass JD. Müller cell cone, an overlooked part of the anatomy of the fovea centralis: hypotheses concerning its role in the pathogenesis of macular hole and foveomacualr retinoschisis. *Arch Ophthalmol* 1999; 117: 821–823.
10 Kishi S, Kamei Y, Shimizu K. Tractional elevation of Henle's fiber layer in idiopathic macular holes. *Am J Ophthalmol* 1995; 120: 486–496.
11 Kishi S, Hagimura N, Shimizu K. The role of the premacular liquefied pocket and premacular vitreous cortex in idiopathic macular hole development. *Am J Ophthalmol* 1996; 122: 622–628.
12 Ito Y, Terasaki H, Suzuki T, Kojima T, Mori M, Ishikawa K *et al*. Mapping posterior vitreous detachment by optical coherence tomography in eyes with idiopathic macular hole. *Am J Ophthalmol* 2003; 135: 351–355.
13 Yanagita T, Shimizu K, Fujimura F, Takano M. Fixation point after successful macular hole surgery with internal limiting membrane peeling. *Ophthalmic Surg Lasers Imaging* 2009; 40: 109–114.
14 Lo D, Heussen F, Ho HK, Narala R, Gasperini J, Bertoni B *et al*. Structural and functional implications of severe foveal dystopia in epiretinal membranes. *Retina* 2012; 32: 340–348.
15 Weinberger D, Stiebel-Kalish H, Priel E, Barash D, Axer-Siegel R, Yassur Y *et al*. Digital red-free photography for the evaluation of retinal blood vessel displacement in epiretinal membrane. *Ophthalmology* 1999; 106: 1380–1383.
16 Shiragami C, Shiraga F, Yamaji H, Fukuda K, Takagishi M, Morita M *et al*. Unintentional displacement of the retina after standard vitrectomy for rhegmatogenous retinal detachment. *Ophthalmology* 2010; 117: 86–92.
17 Machemer R, Steinhorst UH. Retinal separation, retinotomy, and macular relocation: I. experimental studies in the rabbit eye. *Graefes Arch Clin Exp Ophthalmol* 1993; 231: 629–634.
18 Machemer R, Steinhorst UH. Retinal separation, retinotomy, and macular relocation: II. a surgical approach for age-related macular degeneration? *Graefes Arch Clin Exp Ophthalmol* 1993; 231: 635–641.
19 Eckardt C, Eckardt U, Conrad HG. Macular rotation with and without counter-rotation of the globe in patients with age-related macular degeneration. *Graefes Arch Clin Exp Ophthalmol* 1999; 237: 313–325.

20 Aisenbrey S, Lafaut BA, Szurman P, Grisanti S, Lüke C, Krott R *et al*. Macular translocation with 360 degree retinotomy for exudative age-related macular degeneration. *Arch Ophthalmol* 2002; 120: 451–459.
21 Terasaki H, Miyake Y, Suzuki T, Niwa T, Piao CH, Suzuki S *et al*. Change in full-field ERGs after macular translocation surgery with 360° retinotomy. *Invest Ophthalmol Vis Sci* 2002; 43: 452–457.
22 Terasaki H, Ishikawa K, Suzuki T, Nakamura M, Miyake K, Miyake Y *et al*. Morphologic and angiographic assessment of the macula after macular translocation surgery with 360° retinotomy. *Ophthalmology* 2003; 110: 2403–2408.
23 Terasaki H, Ishikawa K, Niwa Y, Piao CH, Niwa T, Kondo M *et al*. Changes in focal macular ERGs after macular translocation surgery with 360 degrees retinotomy. *Invest Ophthalmol Vis Sci* 2004; 45: 567–573.
24 Takeuchi K, Kachi S, Iwata E, Ishikawa K, Terasaki H. Visual function 5 years or more after macular translocation surgery for myopic choroidal neovascularisation and age-related macular degeneration. *Eye* 2012; 26: 51–60.

週刊 Journal of Clinical and Experimental Medicine（IGAKU NO AYUMI） established in 1946
医学のあゆみ
第1土曜特集

Vol.245 No.5
2013
5/4
第245巻・第5号（通巻2950）
2013年5月4日発行（毎週土曜日発行）
昭和21年7月27日第3種郵便物認可
[ISSN 0039-2359 CODEN:IGAYAY]

エクソーム解析
――成果と将来

企画 松本直通 横浜市立大学大学院医学研究科遺伝学

医歯薬出版株式会社
http://www.ishiyaku.co.jp/

医学のあゆみ

エクソーム解析——成果と将来

企画　松本直通　（横浜市立大学大学院医学研究科遺伝学）

第1土曜特集
Vol.245 No.5　2013/5/4

CONTENTS

http://www.ishiyaku.co.jp/

■サイドメモ

全エクソーム解析による遺伝性網脈絡膜疾患の原因遺伝子探索

Investigation genes responsible for inherited retinal diseases by whole exome sequencing

岩田　岳（写真左）　古野正朗（写真中央）　池尾一穂（写真右）
Takeshi IWATA[1], Masaaki FURUNO[2] and Kazuho IKEO[3]
国立病院機構東京医療センター臨床研究センター（感覚器センター）分子細胞生物学研究部[1]，理化学研究所オミックス基盤研究領域[2]，国立遺伝学研究所生命情報DDBJ研究センター[3]

◎ヒトが得る全情報の８割は視覚情報に由来すると考えられており，感覚器官のなかでも眼は重要な働きを担っている．眼の後極部に存在する網膜は，光を電気信号に変換する視細胞とそれに連結する視神経細胞やグリア細胞から構成されており，層状をなしている．とくに視細胞が集中する網膜のほぼ中心に位置する黄斑は，最大限に受光するために凹型となっており，血管や視神経細胞が光路を妨げないような構造となっている．遺伝性網脈絡膜疾患の多くは，視細胞や視神経細胞の機能に関与する遺伝子に変異が生じて発症する場合が多い．病態と遺伝形式別に分類すると，約30種類の遺伝性網脈絡膜疾患に分類され，すでに192遺伝子が報告されている．遺伝性網脈絡膜疾患の日本人患者やその家系を対象とした網羅的な遺伝子解析の研究はきわめて限られており，疾患と遺伝子の関係について十分な情報がない．著者らはこのような状況を少しでも改善するために，遺伝性網脈絡膜疾患の家系を対象とした全エクソーム解析によって網羅的な遺伝子解析を行い，日本人患者に関与する遺伝子の解明を試みた．

Key Word：遺伝性網脈絡膜疾患，網膜，視細胞，黄斑，遺伝子解析，次世代シークエンサー

眼は透明な組織であることから，古くから眼内の病態が観察され，詳細に分類されてきた．さらに，技術的な進歩によって可視光，螢光，赤外線を使った眼底像や，高解像度の網膜断層像（OCT），視機能を記録するための網膜電図（ERG）が発達し，さらに遺伝子情報が加わることによる，より正確な診断が期待されている．眼科の臨床遺伝子研究は20年以上前に，脳回転状網脈絡膜萎縮症（gyrate atrophy）患者におけるオルニチンアミノ転移酵素遺伝子（ornithine aminotransferase）の変異が発見されてからはじまり[1]，その後，網膜色素変性患者におけるロドプシン（rhodopsin）遺伝子変異の発見へと続き[2]，黄斑ジストロフィー，加齢黄斑変性，緑内障，そして近視を含む多くの眼疾患に研究は広がっている．

塩基配列の変化と遺伝子機能への影響は個々の疾患によって異なり，高い相関を示す遺伝子変異のなかには，遺伝子機能が失活するものから全く

サイドメモ　網膜，脈絡膜，黄斑

網膜：眼の後極に存在する視細胞とこれに接続する視神経細胞が面状に並んだ部分．光情報を電気信号に変換し，脳へと信号を伝達する．

脈絡膜：強膜の内側にある血管の豊富な膜で，網膜に酸素や養分を補給し，老廃物を運び出す役割がある．加齢黄斑変性では脈絡膜からの血管から網膜への滲出によって視細胞死に至る．網膜の脈絡膜からの剥離（網膜剥離）によっても，この部分の網膜機能は極端に低下する．

黄斑：網膜の中心部にある直径２mmほどの黄色領域．錐体細胞が集中し，視覚の解像度と色覚を決定するもっとも重要な部位である．

影響しないものもある．近年におけるDNAシークエンス技術の革新的な発展によって，患者とその親族の網羅的な全エクソンや全ゲノムを解読することが可能となり，意図的に選別された遺伝子(候補遺伝子)を解析するスタイルから，網羅的な解析結果から考察するスタイルへと変化している．残念ながら現時点では根本的な治療が困難な疾患が多いが，疾患の原因遺伝子が明らかにされることによって診断の精度向上と治療法開発の基礎的情報が得られると考えられる．

本稿では遺伝性網脈絡膜疾患のエクソーム解析について，著者らの取組みを紹介する．

網膜の構造

角膜，水晶体，そして硝子体を通過した光は網膜に結像する．網膜には光を電気信号に変換するための視細胞とこれに接続する視神経細胞，網膜色素上皮細胞，グリア細胞，そして血管が存在し，複雑な層構造を成している(図1)．厚さがわずか0.1～0.3 mmの網膜は感覚器網膜9層と網膜色素上皮細胞から構成され，感覚網膜は神経細胞の視細胞，双極細胞，水平細胞，アマクリン細胞，神経節細胞に加えて，グリア系細胞と血管系細胞が存在する．検眼鏡的には黄斑は視神経乳頭の中心から4 mm耳側に位置し，直径1.5～2.0 mmの黄色を呈する円周を指し，この中心の直径約0.35 mmが中心窩には神経節細胞と内顆粒層が周囲に位置して浅く陥凹し，無血管で，錐体細胞のみが網膜の表層に位置する構造になっている．

黄斑は魚類にはじまり，爬虫類，鳥類へと受け継がれたが，哺乳類の登場時にはいったん消失し，霊長類で再出現されたことが知られている．錐体細胞は桿体細胞に比べて細胞当りのエネルギー代謝が約8倍あり，ミトコンドリアの数も細胞当りでは20倍も異なることが知られている．すなわち，黄斑の中心は，無血管でありながら活発に代謝・機能を維持しなければならない状況にあり，栄養や酸素の供給が不足すると容易に機能が低下する危険性がある．杆体細胞の機能が失われると暗いところで物が見えにくくなったり(鳥目，夜盲)，視野が狭くなったりするような症状を起こし，錐体細胞が障害されると中心部が見えづらくなったり，色の識別ができなくなったりする(色覚異常)．

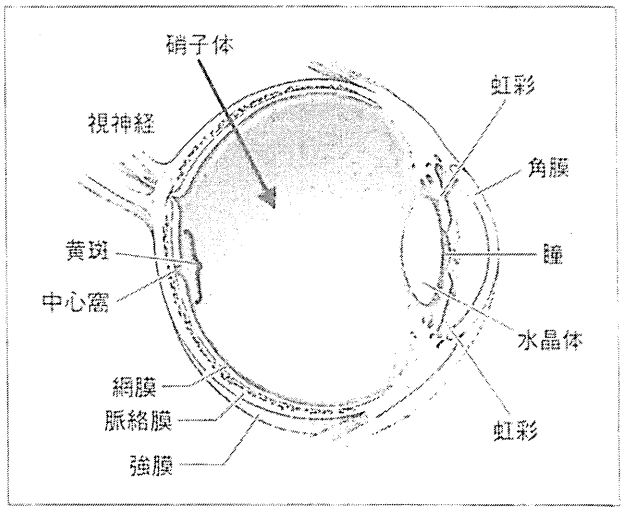

図1　眼球の構造
角膜と水晶体を通過した光は網膜のほぼ中央に位置する黄斑で結像する．中心窩は黄斑の中央に位置し，錐体細胞の密度が網膜中ではもっとも高い．

遺伝性網脈絡膜疾患

遺伝性網脈絡膜疾患はおもに視細胞および網膜色素上皮細胞を病巣としており，①網膜変性，②脈絡膜変性，そして③黄斑変性に大別される．

遺伝性網膜変性には網膜色素変性，錐体ジストロフィー，先天停在性夜盲，白点状網膜症，小口病などがある．とくに網膜色素変性は厚労省によって難病に指定されており，日本には30,000人以上の患者が存在する．もっとも遺伝子解析が進んでいる眼疾患である．遺伝性網脈絡膜変性にはレーバー先天盲，白点状網膜症，脈絡膜ジストロフィー，ミトコンドリア網膜症などがある．さらに，遺伝性黄斑変性には錐体ジストロフィー，錐体-杆体ジストロフィー，Stargardt病，卵黄状黄斑ジストロフィー，先天網膜分離症，オカルト黄斑ジストロフィーなどがある．遺伝性網脈絡膜疾患の原因遺伝子や感受性遺伝子の情報は，Retinal Information Network(RetNet；https://sph.uth.edu/retnet/)で閲覧することができる．疾患の遺伝子座の報告と原因遺伝子や感受性遺伝子の発見は年々増加しており，今後東洋人の解析が進むについて，さらに増加すると予想される(図2)．

黄斑疾患には浮腫，剝離，嚢腫，萎縮などの障害もあり，遺伝以外の要因によって発症する眼疾